Receptor-mediated cell attachment and detachment kinetics
II. Experimental model studies with the Radial-Flow Detachment Assay

Cindi Cozens-Roberts, John A. Quinn, and Douglas A. Lauffenburger
Department of Chemical Engineering, University of Pennsylvania, Philadelphia, Pennsylvania 19104 USA

ABSTRACT   Quantitative information regarding the kinetics of receptor-mediated cell adhesion to a ligand-coated surface are crucial for understanding the role of certain key parameters in many physiological and biotechnology-related processes. Here, we use the probabilistic attachment and detachment models developed in the preceding paper to interpret transient data from well-defined experiments. These data are obtained with a simple model cell system that consists of receptor-coated latex beads (prototype cells) and a Radial-Flow Detachment Assay (RFDA) using a ligand-coated glass disc. The receptors and ligands used in this work are complementary antibodies. The beads enable us to examine transient behavior with particles that possess fairly uniform properties that can be varied systematically, and the RFDA is designed for direct observation of adhesion to the ligand-coated glass surface over a range of shear stresses. Our experiments focus on the effects of surface shear stress, receptor density, and ligand density. These data provide a crucial test of the probabilistic framework. We show that these data can be explained with the probabilistic analyses, whereas they cannot be readily interpreted on the basis of a deterministic analysis. In addition, we examine transient data on cell adhesion reported from other assays, demonstrating the consistency of these data with the predictions of the probabilistic models.

INTRODUCTION

The kinetics of receptor-mediated cell adhesion to a ligand-coated surface play a key role in many physiological and biotechnology-related processes. Biotechnology-related examples described in the preceding paper (hereafter referred to as "Part 1" [1]), include certain cell separation techniques, such as cell affinity chromatography (CAC), and endothelial cell (EC) seeding of prosthetic vascular grafts. In that paper, we discuss the complexity of the cell-to-surface interaction and the adhesion assays typically used to examine attachment and detachment kinetics. These assays have provided useful information on receptor-mediated adhesion kinetics. However, the complexity of the interaction and the difficulty associated with measuring certain key parameters have left many fundamental questions unanswered. In this paper, our objectives are to use the probabilistic models developed in Part 1 to interpret data from well-defined kinetic experiments. We use a model cell system that employs 10-μm diam receptor-coated latex beads (prototype cells) and a Radial-Flow Detachment Assay (RFDA) with a ligand-coated glass surface. The beads enable us to examine transient behavior with particles possessing uniform properties (such as size, shape, and receptor number) that can be varied in a range typical for receptor-mediated cell adhesion (2). The RFDA produces a laminar axisymmetric flow field, providing a continuous range of shear stresses within a given experiment. In addition, the RFDA is designed for direct observation of adhesion to the coated glass disc under both transient and equilibrium conditions, providing time-dependent attachment and detachment data as a function of shear stress (reported on here) as well as equilibrium detachment data (2).

The transient data obtained with our model cells and the RFDA provide a crucial test of the probabilistic framework, along with the use of parameter values that are consistent with previous estimates (2). The experiments reported on here focus on the effects of surface shear stress, receptor density, and ligand density. We show that these data can be interpreted with the probabilistic analyses. They cannot, however, be readily explained with a deterministic analysis. We also examine transient data on EC seeding of prosthetic vascular grafts, CAC, and cell adhesion reported from other assays, demonstrating the consistency of these data with the predictions of the probabilistic models.

NOMENCLATURE

a Contact area radius (μm)
C Number of receptor-ligand complexes

Address correspondence to Prof. John A. Quinn, Department of Chemical Engineering, University of Pennsylvania, 220 South 33rd Street, Philadelphia, PA 19104.

F	Force (dyn)
h	Gap width between discs (mm)
h_s	Separation distance between particle and plate (μm or Å)
H	Maximum distance for receptor-ligand binding (μm or Å)
k_b	Boltzman constant (J/molecule-K)
k_f^0	Forward rate constant (cm^2/min)
k_r	Reverse rate constant under conditions of flow (min^{-1})
k_r^0	Reverse rate constant (min^{-1})
K^0	Affinity constant (cm^2)
L	Plate coating concentration (μg/ml)
N	Surface density (cm^{-2})
p	Probability density function
P	Probability
Q	Volumetric flow rate (ml/s)
r	Radial distance from stagnation point (mm)
Re	Local Reynolds number
R_T	Total number of receptors available for binding within the contact area
t	Time (min)
$t_{1/2}$	Half-life (min)
T	Temperature (K)
S	Shear stress (dyn/cm^2)

Subscripts

a	Attachment
b	Bond
B	Bead
c	Critical
F	Final
L	Ligand
m	Maximum
R	Receptor
T	Total
u	Unstable

Greek characters

α	Dimensionless force
β	$(K^0/33e)(k_b T/\gamma)(a/\rho_B)^3$
γ	Range of the bond interaction (nm)
κ	Dimensionless dissociation constant
λ	S_c for net nonspecific force (dyn/cm^2)
μ	Viscosity (g/cm-s)
ρ	Radius (μm or mm)
θ	Dimensionless bond number
σ^2	Variance
τ	Dimensionless time
ξ	S_c for given t_a divided by that at $t_a = 32$ min
Ψ	Half-life divided by the maximum value for the half-life
ζ	No. of adherent beads after shear divided by no. before shear

MATERIALS AND METHODS

Radial-Flow Detachment Assay

The RFDA used for the present experiments is discussed in previous work (2). Briefly, the RFDA produces a laminar axisymmetric flow field, characterized by a radial decrease in the surface shear stress (S). In fact, S is predicted to be inversely proportional to the radial distance from the central stagnation point (r):

$$S = 3Q\mu/\pi r h^2, \tag{1}$$

where Q is the volumetric flow rate, μ is the viscosity, and h is the gap width between the two discs. Thus, within the inner zone surrounding the stagnation point, shear stresses are higher and the particles are swept away; and within the outer zone, shear stresses are lower and the particles remain attached. The radius that marks the boundary between these two zones defines the critical radius (r_c); the critical shear stress (S_c) is determined by using the value for r_c in Eq. 1. In general, r_c is fairly distinct at low magnifications; however, at higher magnifications, this fairly distinct zone is observed to be graduated with respect to the fraction of adherent beads (ζ), where ζ is the number of adherent beads at some particular time ($t \geq 0$) divided by the number of adherent beads before the initiation of flow (at $t = 0$). As a result, it is difficult to assign a particular value to r_c; hence, by convention, we define r_c to be the radius where ζ is equal to 0.5 (3–6). The RFDA is designed for direct observation of adhesion to the glass surface under both transient and equilibrium conditions and data are recorded with a 35-mm camera.

Plate and bead coating procedures

In the present experiments, as in previous work (2), goat IgG (hereafter referred to as Ag) and rabbit anti-goat IgG (hereafter referred to as Ab) were used to represent the receptor-ligand system. The plate and bead (carboxylated latex microsphere) coating procedures and the procedures for determining the coating densities have been described (2). Briefly, beads were coated with receptors by means of carbodiimide chemistry, which covalently binds the receptor via an amine group to an activated carboxylate group on the sphere. Plates were treated with 3-aminopropyltriethoxysilane to form an alkylamine carrier, then ligand was covalently coupled to the surface by means of glutaraldehyde chemistry, which attaches the ligand via an amine group to an aldehyde group on the plate. Ethanolamine and glycine were used to block unreacted sites on the beads and plates, respectively. Effective receptor numbers and ligand densities are estimated from total receptor numbers and ligand densities by making several assumptions. These assumptions account for the loss in activity of the molecules due to the coupling procedure and the polyclonal nature of the antibody. We estimate that the effective Ab density is equal to 0.063 times the total Ab density and the effective Ag density is equal to 0.32 times the total Ag density (2). Cress and Ngo (7) measured the specific binding capacity of rabbit anti-human IgG immobilized to a surface via its amine groups and obtained a value of 0.06 mg human IgG per mg rabbit IgG, in excellent agreement with our predictions for Ab.

Procedure for attachment experiments

For the present experiments, the feed solution was 0.01 M potassium chloride (KCl) in treated water (passed through two deionizers, a carbon tank, and a 0.22-μm filter), with a pH of 6.6. To start an

experiment, the chamber was assembled, then inverted, and 0.3 ml of bead solution was slowly injected into the RFDA through a three-way valve in the inlet line (2). The beads were incubated with the affinity surface for a specified time of either 4, 5, 15, 30, or 43 min. The chamber was placed on the stage, requiring inversion with attendant fluid motion sufficient for detachment of any loosely "attached" beads. Pictures were taken of adhesion at three different regions of the ligand-coated disc to provide data on the initial number of beads per square centimeter. As a result, there was a time lag from inversion of the chamber (to place it on the stage) to the initiation of flow. For consistency, this time period was fixed at 2 min. The beads were exposed to a constant volumetric flow rate for 30 min (shear times are typically on the order of 10–30 min in cell adhesion assays [6, 8–11]), after which r_c was measured from the average of four different readings of the stage x-y displacement from the central stagnation point (2 Δx and 2 Δy readings). Pictures were taken across a radius of the disc to provide data for ζ as a function of S. The photographs are at a magnification of 95 and span a 0.8 by 1.2-mm region of the coated disc (~9% of the total relevant radius). In general, each attachment time for each receptor and ligand coating combination was run in duplicate or triplicate.

Procedure for detachment experiments

The procedure for these experiments is similar to that for the attachment time experiments with three exceptions. First, beads were incubated with the affinity surface for 30 min (plus, for consistency, 2 min from the time of inversion of the chamber to place it on the stage to the start of flow). Second, region(s) of the ligand-coated glass plate were photographed before exposure to shear (taken as $t = 0$) until $t = 60$ min. These pictures are of either a single region of the plate or of several overlapping regions of the plate. They are at a magnification of 76 or 95 and span a 1.0 by 1.5-mm or 0.8 by 1.2-mm region of the coated disc, respectively. This region(s) is divided into "shear stress zones," each zone is assigned an average value of S, typically an integer value with a range of $S \pm 0.5$ dyn/cm². The value of ζ in each zone is determined with respect to time. Data are considered satisfactory if they meet the "steady-state" criterion for detachment. This criterion is that <2 beads per 100 detach from $t = 45$ to $t = 60$ min (<2% detachment in the final 15 min).

MATHEMATICAL ANALYSIS

In this section, we review the expressions for the total fluid force (F_T) exerted on an adherent particle at a given radial position in the RFDA, the number of bonds required for adhesion at the critical radius (r_c), and the critical shear stress (S_c) as a function of several key parameters, such as the receptor and ligand densities. In addition, we discuss the adaptations required for the interpretation of RFDA data with the analyses developed in Part 1 (1).

Fluid and adhesion-related forces

The following expressions, applicable to receptor-mediated particle adhesion in the RFDA, are derived in detail in previous work (2) and are based on the theoretical framework of Bell (12) and of Hammer and Lauffenburger (13).

The total force (F_T) exerted by the passing fluid on an adherent bead at a given radial position is estimated to be:

$$F_T \approx 110 S \rho_B^3 / a, \tag{2}$$

where ρ_B and a are the radius of the bead and the contact area, respectively. The total force at r_c is determined by using the value for S_c in Eq. 2. We estimate the number of receptor-ligand complexes (C) required for adhesion at S_c with the following expression (2):

$$C = [160\gamma/k_b T] [S_c/(\ln(K^\circ N_L))] [\rho_B^3/a], \tag{3}$$

where γ is the range of the interaction (~0.5 nm for an antigen-antibody bond [12]), k_b is the Boltzman constant, K° is the receptor-ligand affinity constant, N_L is the ligand density, and T is the temperature. The expressions in Eqs. 2 and 3 are based on the assumptions that the contribution from the nonspecific forces to the adhesive force is negligible and the bonds are equally distributed and stressed.

The following expression was developed for S_c:

$$S_c \approx \beta N_L N_R + \lambda, \tag{4}$$

where: $\beta = (K^\circ/33e)(k_b T/\gamma)(a/\rho_B)^3$; and λ is the critical shear stress that would be measured in the absence of specific forces. For $\lambda = 0$ (a negligible nonspecific adhesive force), Eq. 4 predicts that S_c is linearly proportional to N_L, N_R, and β, where β is linearly proportional to K° and $(a/\rho_B)^3$. The models developed in Part 1 (1) also predict an increase in the adhesive force with an increase in N_L, N_R, and/or K°. In previous work (2), we demonstrated experimental validation of the expression in Eq. 4, and showed it to be consistent with reasonable estimates for K°. In addition, we showed that $\lambda \approx 0$ for the interaction between Ab-coated beads and Ag-coated plates.

Adaptation of probabilistic models for analysis of RFDA data

In Part 1 (1), we define the following dimensionless parameters:

$$\theta = C/R_T \quad \tau_a = k_f^\circ N_L t_a \quad \tau = k_f^\circ N_L t$$

$$\kappa = k_r^\circ/k_f^\circ N_L \quad \alpha = [\gamma/k_b T R_T] F_T,$$

where θ is the dimensionless bond number, τ_a is the dimensionless attachment time, τ is the dimensionless time, κ is the dimensionless dissociation constant, α is the

dimensionless force acting on the bonds, R_T is the total number of receptors available for binding within the contact area $(R_T = \pi a^2 N_R)$, and k_f^o and k_r^o are the forward and reverse rate constants, respectively. The expression for α at a given radial position in the RFDA is obtained by substituting the expression for F_T (Eq. 2) into the definition for α:

$$\alpha \approx [110\gamma\rho_B^3/k_b Ta][S/R_T]. \tag{5}$$

This expression predicts that, for a given α at constant a, ρ_B, T, and γ, S is linearly proportional to R_T.

In our analyses (1), we focus on the role of receptor-ligand kinetics in yielding deviations from ideal, deterministic behavior because most kinetic data do not follow the deterministic solution exactly, but fluctuate about it. This is especially true when the number of reacting molecules is relatively small as is the case with the receptors on our model cells (see Table 1). Deviations from ideal behavior may, however, also result from heterogeneous properties, such as the receptor/ligand affinity constant and the number of ligand and the number of receptor molecules available for binding within the contact area. We assume that the Ag/Ab interaction can be represented by a single affinity constant and the number of Ab and of Ag available for binding within the contact area can be represented by single numbers. The extent to which these assumptions are valid is discussed in Appendix 1, where we compare the contribution of the Ag/Ab kinetics in yielding deviations from deterministic behavior with the net contribution of the heterogeneous properties. We show that the net contribution from heterogeneous properties is about an order of magnitude smaller than that of the kinetics, explaining our focus on the kinetics. In addition, in Appendix 1, we present a qualitative argu-

ment that the deterministic model could not predict the instantaneous detachment seen with our model cells (see Fig. 3) and predicted by the probabilistic analysis (Part 1 [1], Fig. 8) if it were modified to account for heterogeneous properties, i.e., only the kinetics can account for this behavior.

Three additional assumptions are made in our analyses. First, we assume that the ligand density is much greater than the receptor density; so, the ligand density is approximately constant. In the experiments reported on here, the Ag density is estimated to be 3.8–16 times the Ab density (see Table 1); therefore, we assume that the Ag density is approximately constant, while recognizing that rigorous modeling of these data would treat the Ag density as variable. As a result, the ligand density remains constant if Ag is coupled to the glass disc, and the receptor density remains constant if Ag is coupled to the beads. The analysis for constant receptor density is similar to that for constant ligand density, the receptor and ligand densities are simply interchanged in the model equations. Second, the distribution of complexes is assumed to be homogeneous. Our third simplifying assumption is that there is a constant number of total receptors in the contact area; for our bead model "cells," this is clearly the case because there is no receptor mobility.

It is theoretically possible to predict the probability of detachment for a single value of shear stress, i.e., the detachment in a region of infinitesimal width. It is, however, impossible to obtain experimental data for such a region; consequently, data are obtained for "shear stress zones" (see Materials and Methods). Each zone is assigned the average value of S, typically an integer value with a range of $S \pm 0.5$ dyn/cm^2. Here, for consistency with the experimental data, the model predictions for detachment are grouped into similar shear stress zones.

TABLE 1 **Data from attachment and detachment experiments**

Bead	Receptor	R_{TB}^*	$N_R^\ddagger$	L	$N_L^\ddagger$	S_c	S_m
			cm^{-2}	$\mu g/ml$	cm^{-2}	dyn/cm^2	dyn/cm^2
Attachment							
CM	Ab	6.6×10^6	1.3×10^{11}	5.7	4.9×10^{11}	$10^\S$	—
CN	Ab	3.0×10^6	6.0×10^{10}	5.7	4.9×10^{11}	$4.5^\S$	—
Detachment							
CK	Ab	3.5×10^6	7.0×10^{10}	13	1.1×10^{12}	11	10
CM	Ab	6.6×10^6	1.3×10^{11}	5.7	4.9×10^{11}	10	10
CR ($a\&b$)	Ab	7.3×10^6	1.5×10^{11}	5.7	4.9×10^{11}	11	11
CP	Ag	6.4×10^6	6.5×10^{11}	5.5	9.3×10^{10}	16	15
				9.6	1.6×10^{11}	22	22

*Measured values of total receptor number/bead (active plus inactive)
$\ddagger$Estimated active densities (2)
$\S S_c(t_a = 32$ min)

RESULTS AND DISCUSSION

This section contains our transient attachment and detachment results for the interaction between receptor-coated latex beads (prototype cells) and ligand-coated glass plates in the RFDA. These data are interpreted with the probabilistic models developed in Part 1 (1). The experiments focus on the effects of surface shear stress, receptor density, and ligand density. These data are easily explained with the probabilistic analyses. It is, however, difficult to interpret these data with a deterministic analysis. We also examine transient data on EC seeding of prosthetic vascular grafts, CAC, and cell adhesion reported from other assays, demonstrating the consistency of these data with the predictions of the probabilistic models.

RFDA data on model cell attachment

Attachment experiments were performed with Ab-coated beads and plates coated with a 5.7-μg/ml solution of Ag (see Table 1). Two bead types were used, CM and CN, where CM had approximately twice the receptor density as CN. We define: $\xi = S_c(t_a)/S_c(t_a = 32 \text{ min})$. $S_c(t_a = 32 \text{ min}) = 10$ dyn/cm^2 for CM, and $S_c(t_a = 32 \text{ min}) = 4.5$ dyn/cm^2 for CN, where S_c is the shear stress at which 50% of the beads remain attached. Inherent in the probabilistic (and deterministic) attachment analysis is the assumption that the rate of bond formation is significantly slower than the rate of increase in the contact area; therefore, the contact area reaches steady state well before the kinetics and can be treated as a constant. As a result, for the adhesion of a given bead type to a given surface, θ is predicted to be linearly proportional to S_c (see Eq. 3). Therefore: $\xi = S_c(t_a)/S_c(t_a = 32 \text{ min}) = \langle \theta \rangle(t_a)/\langle \theta \rangle(t_a = 32 \text{ min})$, where $\langle \theta \rangle$ is the mean value of θ predicted by the probabilistic attachment model. The probabilistic results for $\langle \theta \rangle$ are identical to the deterministic results for θ (1). The deterministic model does not allow for fluctuations about the mean solution; therefore, it predicts that all of the beads remain adherent at the low range of shear and all of the beads detach at the high range of shear. It is, therefore, difficult to interpret data for S_c (and ξ) with a deterministic analysis because of its "all-or-none" charcter.

Data and probabilistic model results for ξ as a function of t_a are shown in Fig. 1. The probabilistic analysis is for $\kappa = 0.029$. Order of magnitude estimates for N_L, K°, k_r°, and k_f° relevant to our particular experimental system are discussed in Appendix 2. Briefly, N_L is estimated from the ligand concentration of the coating solution, K° is estimated using equilibrium detachment data (2), and k_r° and
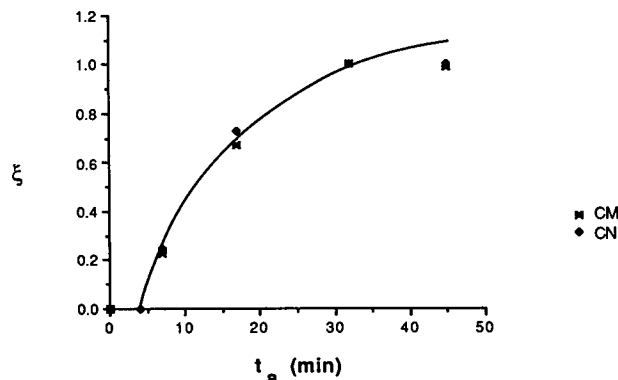

FIGURE 1 Data and probabilistic model predictions for the effect of attachment time (t_a) on the critical shear stress, where ξ is the critical shear stress at a given t_a divided by that at $t_a = 32$ min (defined to be equal to the mean value of the dimensionless bond number [$\langle \theta \rangle$] at a given t_a divided by that at $t_a = 32$ min). Data shown are for two bead types, CM and CN (Table 1), and the experiments were run in duplicate or triplicate. Probabilistic results shown here are for $\kappa = 0.029$, $k_f^\circ N_L = 0.070$ min^{-1}, and $k_r^\circ = 0.0020$ min^{-1} with a 4-min time lag imposed by subtracting 4 min from the value of t_a.

k_f° are fit from the kinetic attachment and detachment data presented here; in addition, these estimates are shown to be consistent with values from the literature. In general, the data and analysis are in excellent agreement. The data do, however, show a 4-min time lag before the development of a stable adhesive force, i.e., for $t_a \leq 4$ min, over 50% of the beads detach from the coated surface when the RFDA chamber is inverted to place it on the stage, a result of attendant fluid motion (plus gravity). (Note that since we allow 2 min from chamber inversion to start up, 2 min are added to incubation times of 5 min or greater to yield the final value of t_a). This time lag is not predicted by the model (see Part 1 [1], Fig. 2), the 4 min time lag in the model results presented in Fig. 1 is imposed by subtracting 4 min from the value for t_a, i.e., $\tau_a = (t_a - 4)k_f^\circ N_L$. The model does not allow for this time lag because the receptors and ligands are assumed to be in binding proximity at $t_a = 0$. This assumption is, however, not realistic for the RFDA due to the settling time required for the beads to reach the coated surface after they are injected into the chamber. We can estimate from theory that this settling time can range from negligible to on the order of a few minutes, depending on the starting location of the bead within the gap between the two discs of the RFDA (see Appendix 3). In addition, another contribution to the time lag could be an energy barrier for adhesion. Such a barrier would be the result of repulsive nonspecific forces that could prevent immediate establishment of the contact area, i.e., a small enough gap width

(h_s) between the bead and surface for complex formation (14, 15).

An increase in the contact area and/or an increase in the number of bonds is predicted to increase S_c (see Eq. 3). Therefore, the data for ξ as a function of t_a can be attributed to the rate of increase in the contact area and/or the rate of bond formation. The beads are produced by a linear polymerization of polystyrene, whose characteristic hydrophobic interactions provide resistance to both elastic and plastic deformation (2). A time-dependent increase in the contact area cannot, therefore, be attributed to "spreading" of the beads on the surface. In previous work (2), we modeled the contact area as a function of two parameters: h_s, the separation distance between the bead and plate; and H, the maximum distance for receptor-ligand binding. We found that the contact area increases as h_s decreases and/or H increases. Although H is varied in the model, it should be a constant in a given medium; therefore, h_s would be the only parameter that might vary within a given experiment. Hence, the only way that the contact area could increase with time would be if h_s decreased with time, which is unlikely because h_s should be limited by a repulsive steric stabilization force (16). Steric stabilization forces result from the overlapping of molecules on opposing surfaces, and arise from both the change in environment of these molecules as well as their conformational restrictions due to the presence of neighbors. In general, this force is repulsive and of greater magnitude than the other nonspecific forces (16). Therefore, the overlapping of these molecules acts almost as a barrier, restricting the gap width between the two surfaces to a distance small enough for Ag/Ab binding yet large enough that Ag/Ab overlap is insignificant. It would, therefore, seem more reasonable that the rate-limiting step for bead attachment would be the rate of bond formation. The similarity between the RFDA data and attachment analysis supports this hypothesis.

The data shown in Fig. 1 are not a function of the receptor number per bead (R_{TB}), where $R_{TB} = R_T \cdot (4\rho_B^2/a^2)$, because they are presented in dimensionless form (are normalized with respect to R_T). Probabilistic results for $\langle\theta\rangle$ and, therefore, for ξ are also not a function of R_T for $R_T \gg 10$ because the dimensionless parameter δ, where $\delta = R_T^{-1}$, is negligible (see Part 1). S is predicted to be linearly proportional to R_T (Eq. 5); therefore, the steady state value of S_c should increase linearly with R_{TB}. This is also consistent with the behavior predicted by Eq. 4, where $\lambda \approx 0$ for the interaction between Ab-coated beads and Ag-coated plates (2). These data do, in fact, show approximately a proportional increase in the value of S_c with R_{TB}, for $t_a \geq 32$ min: $S_c = 10$ dyn/cm^2 for CM

with $\sim 6.6 \times 10^6$ total Ab/bead; and $S_c = 4.5$ dyn/cm^2 for CN with $\sim 3.0 \times 10^6$ total Ab/bead (see Table 1).

## RFDA data on model cell detachment

In this section, unless otherwise stated, the parameter values used for the probabilistic analyses of experiments with Ab-coated beads are $\kappa = 0.029$, $k_f^0 N_L = 0.070$ min^{-1}, $k_r^0 = 0.0020$ min^{-1}, $\gamma = 0.5$ nm, $T = 296$ K, $R_T = 1,300$, $\rho_B = 4.8$ μm, and $a = 0.5$ μm. The results as presented (in dimensionless form) are not a function of R_T because for a given α at constant a, ρ_B, T, and γ, S is linearly proportional to R_T (see Eq. 5). Therefore, a change in R_T simply changes the value of S used in the analyses. A constant value is, however, chosen for consistency with the experiments.

In the RFDA detachment experiments presented here, we used a 32-min attachment time before exposure to shear. This value of t_a was chosen for the following reasons. The data in Fig. 1 suggest that equilibrium binding is attained by ~ 32 min; a 30 min incubation is frequently used in CAC when the ligand is an antibody (8, 17, 18) and in detachment assays (6, 9); and it is desirable to seed a graft during the period of time required for a vascular implantation procedure, which is typically 30 min (19). In the probabilistic analysis of detachment, the initial probability distribution is evaluated at $\tau_a = 2.0$, which yields $t_a = 28$ min, appropriate for a 32-min attachment time with a 4-min time lag for attachment (see Fig. 1). Our theoretical computations for probabilistic attachment in Part 1 (1) yield a probability distribution with a mean bond number ($\langle\theta\rangle$) of 0.84 and variance (σ^2) of 0.13 at $\tau_a = 2.0$. We use a lognormal distribution with these properties for our detachment initial condition.

Fraction of adherent beads (ξ) as function of shear stress and time

Detachment data were obtained with three different Ab-coated bead types (CK, CM, or CR) and ligand (Ag) coating concentrations of either 5.7 (CM and CR) or 13 μg/ml (CK) (see Table 1). Typical detachment results and derived data are shown in Figs. 2 and 3, respectively, for bead type CR and plates coated with a 5.7-μg/ml solution of Ag. Fig. 2 consists of a series of photographs that show the time-dependent nature of detachment, and Fig. 3 shows a plot of ξ vs. t at different S. The probabilistic detachment model predicts the probability of having bonds (P_b), where we define P_b to be equal to the probability of remaining attached; therefore, P_b is equivalent to ξ. These data are identical in qualitative form to the probabilistic model predictions for the effect of the
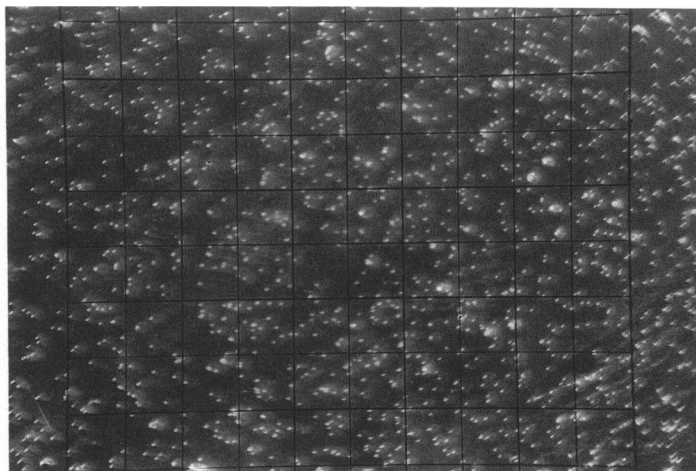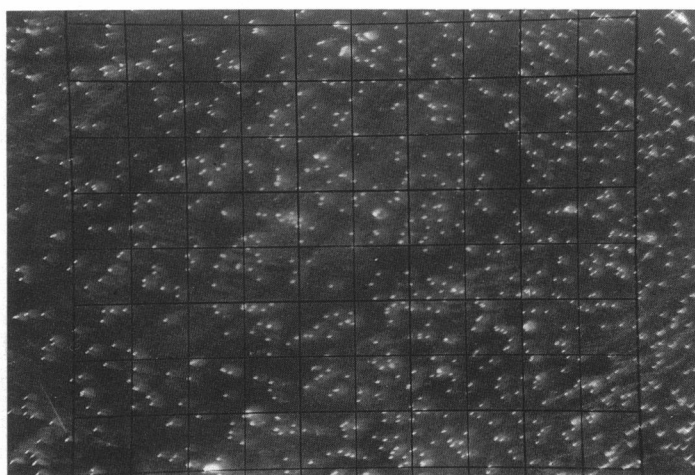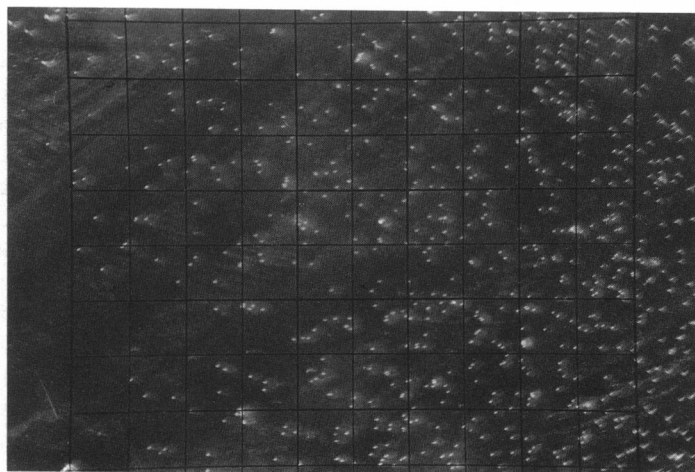
FIGURE 2   RFDA detachment results (dark field image) for Ab-coated beads (CR) and plates coated with a 5.7-μg/ml solution of Ag. These photographs are centered at a radial position of ~5.5 mm, and a shear stress of ~11 dyn/cm^2. (a) Adhesion at 0 min (before the start of flow); (b) 1.6 min; and (c) 27 min. The magnification is 76; the distance between adjacent grid lines is 120 μm.
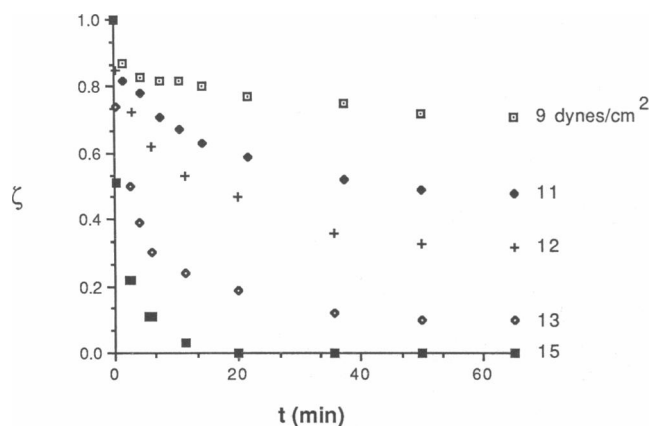
FIGURE 3 A plot of the fraction of adherent beads (ζ) vs. time at various values of shear stress. Data shown are for Ab-coated beads (CR) and plates coated with a 5.7-μg/ml solution of Ag.
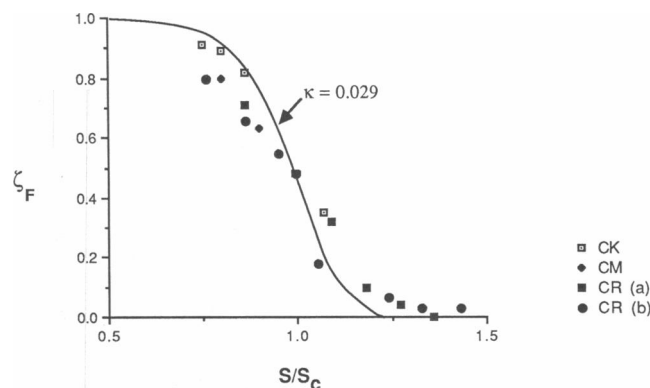

FIGURE 4 Data and predictions of the probabilistic model and of the deterministic model for the effect of the dimensionless shear stress (S/S_c) on the final fraction of adherent beads (ζ_F), where S_c is the shear stress at which $\zeta_F = 0.5$. These data are from four experiments with Ab-coated beads and Ag-coated plates. Each experiment was performed with one of three bead types (CK, CM, or CR) and ligand coating concentrations of either 5.7 (CM and CR) or 13 μg/ml (CK) (Table 1). Probabilistic results are for $\kappa = 0.029$, $k_f^0 N_L = 0.070$ min^{-1}, and $k_r^0 = 0.0020$ min^{-1}; the initial distribution is lognormal with $\langle \theta \rangle = 0.84$ and $\sigma^2 = 0.13$.

dimensionless force (α) on detachment (see Part 1 [1], Fig. 8). These data can, therefore, be interpreted with the probabilistic analysis (see Part 1 [1]). These data cannot, however, be readily interpreted with the deterministic analysis of detachment, which predicts that all of the beads are adherent at the low range of shear and all of the beads detach at the high range of shear, and that all of the beads at a given S detach at the same value of the dimensionless time (τ) rather than over a range of τ (see Part 1 [1], Fig. 6).

"Final" value of ζ

From Fig. 3, we see ζ_F (the "final" fraction of adherent beads) is a function of S. As mentioned in the previous section, P_b is analogous to ζ; therefore, $P_{b(F)}$ is analogous to ζ_F. In Fig. 4, we show ζ_F as a function of S/S_c for the four sets of Ab-coated bead data described in the previous section and for the probabilistic and deterministic model predictions. For the RFDA, S/S_c increases as r decreases (Eq. 1). By definition, $\zeta_F = 0.5$ at $S/S_c = 1.0$; therefore, all four sets of data contain this point. As expected, these data are consistent with the probabilistic model predictions for $P_{b(F)}$ as a function of S/S_c. These data are, however, difficult to explain with the deterministic analysis which predicts that the detachment curve for ζ_F as a function of S is a step function with $\zeta_F = 1.0$ at the lower range of S and $\zeta_F = 0$ at the higher range of S. In addition, these dimensionless data are not greatly effected by a two-fold increase in N_L (consistent with the probabilistic analysis, see Part 1 [1], Fig. 9) or by a change in R_{TB} (predicted by the analysis).

Half-life for ζ

Because the value for ζ becomes fairly constant for longer times, we characterize detachment data in terms of its

half-life ($t_{1/2}$), where $t_{1/2}$ is defined as the time required to reach half of the "final" detachment value. For example, in Fig. 3, $\zeta_F = 0.5$ for $S = 11$ dyn/cm^2; so, $t_{1/2}$ is the time required to reach $\zeta = 0.75$, which is ~6.0 min. In Part 1 (1), we define the dimensionless half-life, Ψ. Here, because we assume that $k_f^0 N_L$ is constant, we define: $\Psi = \tau_{1/2}/\tau_{(1/2)m} = t_{1/2}/t_{(1/2)m}$; and $S_m = S(t_{(1/2)m})$, where $t_{(1/2)m}$ is the maximum value for $t_{1/2}$. For the RFDA, S/S_m increases as r decreases. Fig. 5 illustrates the effect of S/S_m on Ψ for the probabilistic model analysis and for the four sets of Ab-coated bead data described in the previous sections. By definition, $\Psi = 1.0$ at $S/S_m = 1.0$; therefore, all four sets of data contain this point. All four sets of data also contain the point (0, 0) (not shown). This point reflects the fact that none of the beads detach ($t_{1/2} = 0$) when the chamber is inverted (S/S_m small). In other words, because none of the beads detach at $S \approx 0$, ζ_F is attained instantaneously. The probabilistic analysis is consistent with these data, except for CK at $S/S_m \approx 0.85$. The data for CK are for a ligand coating concentration of 13 μg/ml, whereas the other data are for a ligand coating concentration of 5.7 μg/ml. As N_L increases, the model predicts that Ψ decreases for α/α_m (S/S_m) between ~0.6 and 1.0, and Ψ is not a strong function of N_L for S/S_m between 1.0 and 1.4 (see Part 1 [1], Fig. 10). Therefore, in Fig. 5, Ψ for CK are predicted to be smaller than Ψ for CM and for CR at $S/S_m < 1.0$, and to be similar to Ψ for CM and for CR at $S/S_m > 1.0$. The CK data are, in fact, somewhat similar to the model results for $\kappa = 0.017$, i.e., for a commensurate increase in N_L (see Part 1 [1], Fig.
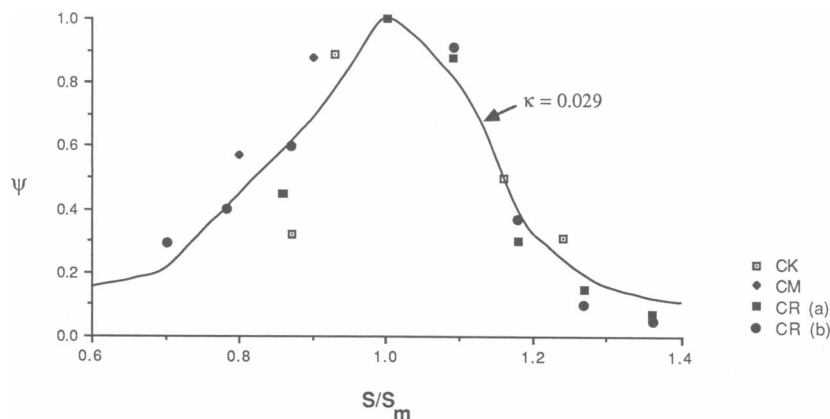
FIGURE 5 A plot of the data and probabilistic model predictions for dimensionless half-life (Ψ) as a function of dimensionless shear stress (S/S_m) (where S_m is the shear stress at which the half-life is maximal). The data are from four experiments with Ab-coated beads and Ag-coated plates. Each experiment was performed with one of three bead types (CK, CM, or CR) and ligand coating concentrations of either 5.7 (CM and CR) or 13 μg/ml (CK) (Table 1). Here, $\kappa = 0.029$, $k_f^o N_L = 0.070$ min^{-1}, and $k_r^o = 0.0020$ min^{-1}; the initial distribution is lognormal with $\langle \theta \rangle = 0.84$ and $\sigma^2 = 0.13$.

10). In addition, these dimensionless data are not a strong function of R_{TB}, consistent with the analysis.

Detachment with a nonspecific adhesive force

S_c is predicted to be a function of β, N_L, N_R, and λ, where λ is the critical shear stress that would be measured in the absence of a specific adhesive force (Eq. 4). The RFDA equilibrium detachment data presented in previous work (2) for this Ag/Ab system show that β is a constant; however, λ is ~0 for the interaction between Ab-coated beads and Ag-coated plates and ~4 dyn/cm^2 for the interaction between Ag-coated beads and Ab-coated plates. These values of λ are consistent with those measured in previous work (2) for the nonspecific interaction between glycine-coated plates and Ab-coated beads and Ag-coated beads, respectively, where glycine is used to deactivate remaining aldehyde groups on the ligand-coated surface (see Materials and Methods). A key assumption in the probabilistic (and deterministic) detachment model is that the net contribution of the nonspecific forces to the adhesive force is negligible. This assumption is, therefore, valid for the Ab-coated bead/Ag-coated plate interaction, but not valid for the Ag-coated bead/Ab-coated plate interaction. In this section, we use our probabilistic model to analyze detachment data for Ag-coated beads (CP) and plates coated with either a 5.5- or a 9.6-μg/ml solution of Ab (Table 1). These data enable us to compare detachment behavior for a net attractive nonspecific and a specific adhesive force with that for a specific adhesive force only. The parameter values used for the probabilistic analysis are identical to those used to analyze the Ab-coated bead experiments with the following exceptions: $k_f^o N_R$ is substituted for $k_f^o N_L$ (the value is

held at 0.070); and $N_L \pi a^2$ is substituted for R_T (the value is held at 1,300). These substitutions are made because the Ag density is the density that is held constant and Ag is now the receptor vs. the ligand. In addition, as for the analysis of Ab-coated bead experiments, the initial probability distribution ($p[\theta, 0]$) is assumed to be lognormal with $\langle \theta \rangle \approx 0.84$ and $\sigma^2 \approx 0.13$. (Note: the model results shown in Fig. 6, a and b are the same as those shown in Figs. 4 and 5, respectively, because N_L is simply substituted for N_R and vice versa.)

Plots of ζ vs. t for the Ag-coated bead experiments show the same five trends predicted by the probabilistic analysis (see Part 1 [1], Fig. 8) and seen in Fig. 3 (Ab bead data). However, in general, the Ag-coated bead data have greater initial detachment rates at all values of S, and smaller ζ_F at $S < S_c$ (data not shown). In Fig. 6 a, we present probabilistic detachment predictions and Ag-coated bead data for ζ_F as a function of S/S_c. These data are similar in form to the model predictions; however, as mentioned, ζ_F is typically smaller for the Ag-coated beads at $S/S_c < 1.0$. In addition, these dimensionless data show that ζ_F is not a function of the Ab (now the ligand) coating density, consistent with the analysis of this system. In Table 1, however, we see that the specific contribution to the adhesive force is approximately linearly proportional to the ligand coating density [(22 dyn/cm^2 – 4 dyn/cm^2)(5.5/9.6) + 4 dyn/cm^2 $\approx$ 14 dyn/cm^2], as predicted by this model. In Fig. 6 b, we show the change in Ψ with S/S_m for the probabilistic detachment analysis and for the Ag-coated bead experiments. When these data are compared with the probabilistic analysis, we see that: for $S/S_m < 1.0$, Ψ is greater for the Ag-coated beads; and for $S/S_m \geq 1.0$, Ψ is approximately the same. In addition, these dimensionless data show that Ψ is not a function of
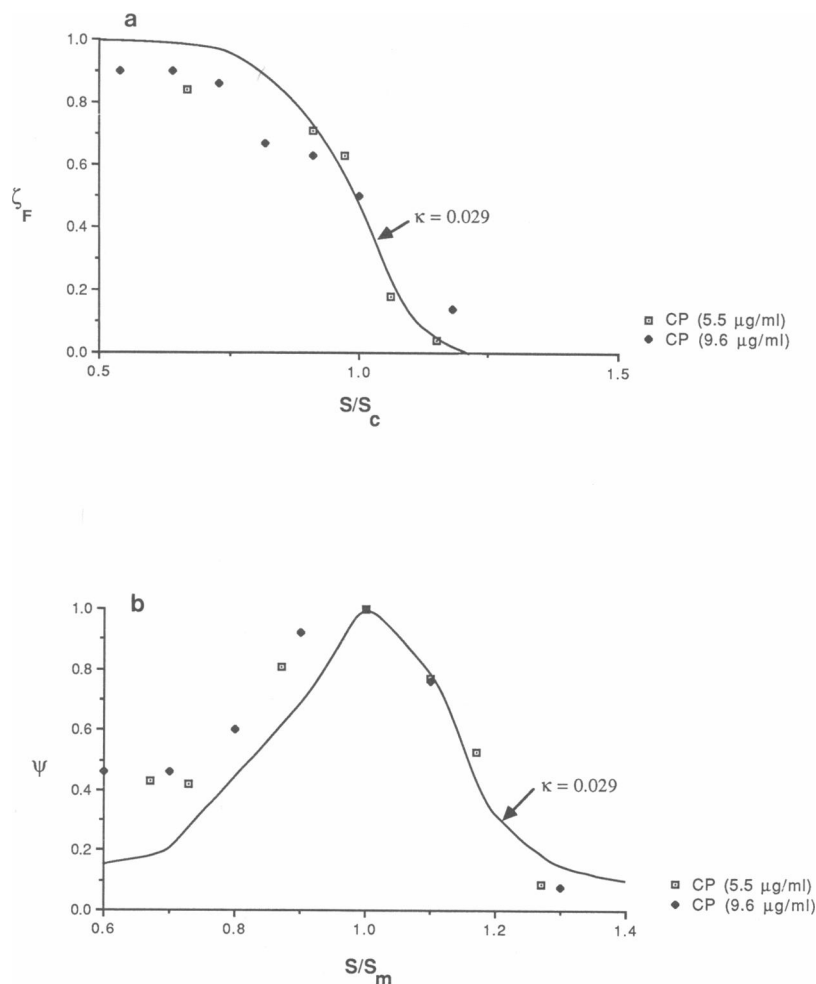
FIGURE 6 (a) A plot of the final fraction of adherent beads (ζ_F) vs. the dimensionless shear stress (S/S_c) (where S_c is the shear stress at which $\zeta_F = 0.5$) for data and probabilistic model results. These data are for Ag-coated beads (CP) and plates coated with either a 5.5 or a 9.6 μg/ml solution of Ab (Table 1). (b) A plot of the change in Ψ with the dimensionless shear stress (S/S_m) (where S_m is the shear stress at which the half-life is maximal) for the probabilistic model analysis and for the Ag-coated bead experiments. The analysis shown is for $\kappa = 0.029$, $k_f^0 N_R = 0.070$ min^{-1}, $k_r^0 = 0.0020$ min^{-1}, and a lognormal initial distribution with $\langle \theta \rangle = 0.84$ and $\sigma^2 = 0.13$.

the Ab coating density, consistent with the analysis of this system. The data in Table 1 show, however, that S_m increases as the ligand coating concentration increases, which is in agreement with model predictions.

Fig. 6, a and b show that the Ab-coated bead data, Ag-coated bead data, and probabilistic detachment analysis behave similarly for S/S_c and for $S/S_m \geq 1$; however, the Ag-coated beads show different detachment behavior for S/S_c and for $S/S_m < 1$. The probabilistic model should, therefore, be modified to accurately predict the detachment behavior over the full range of shear stress examined when the nonspecific adhesive force is significant. This modification must account for the fact that, in order for a particle to detach, all of the bonds must break *and* the nonspecific force must be disrupted.

Comparison with data on cell adhesion

In the RFDA experiments reported on here, we have examined the transient attachment and detachment behavior of receptor-coated latex beads (prototype cells) to and from ligand-coated glass surfaces. The beads enable us to examine the effect of various parameters on transient attachment and detachment behavior with particles possessing fairly uniform properties that can be varied systematically. This system yields reproducible, quantitative results that can be analyzed without consideration of the heterogeneity that is typical of cells. For example, with cells, in general, one must consider heterogeneous cell properties, such as receptor number and class

(17, 20, 21), and heterogeneous surface properties, such as the presence of several different proteins that each interact with unique cell receptors (8, 17, 18, 22, 23). These heterogeneities add to the nonideal nature of cell adhesion behavior. Our model cell system is, therefore, the ideal system to use to test the probabilistic framework developed in Part 1 (1). Our ultimate goal is, however, to analyze data on cell attachment and detachment in the RFDA with our probabilistic models. The interpretation of cell data may be somewhat different than that of bead data not only due to the potential role of heterogeneous properties but also because cells and beads have different properties. For example, on cells, receptors can diffuse into the contact area with attachment time (24, 25), rather than being fixed to the surface; cells may modulate receptor number in response to the environment (20), rather than maintaining a fixed receptor number; and cells can settle onto surfaces and flatten, increasing the contact area between the cells and the surface (26–28), rather than being resistent to deformation. Nevertheless, cell adhesion data from specific applications and from other adhesion assays have shown behavior similar to that predicted by the probabilistic models. We discuss these similarities in the following sections.

Attachment

Data from several different cell attachment assays (see Table 2) show similar behavior to that seen in the RFDA data and in the probabilistic analysis of attachment (Fig. 1). For example, several investigators have found that the adhesive force increases with time at shorter times (6, 9, 10, 19, 26, 29–34); the rate of increase in the adhesive force decreases with time, reaching a constant value (steady state) at longer times (6, 10, 19, 26, 29, 31–34); and there is time lag for adhesion (9, 29–31). These observations include those for EC adhesion to various substrates (9, 19, 26), useful in that they provide information for EC seeding of vascular prosthetic grafts. These data also include CAC attachment results for tissue culture cells (32), mouse bone marrow cells (33), and thymocytes (34).

A decrease in κ due to an increase in N_L is predicted to increase the initial rate of bond formation (adhesive force), yielding a greater bond number at a given t_a; decrease the t_a at which steady state is reached; and increase the steady state value of the bond number (see Part 1 [1], Fig. 4). Weigel et al. (29) examined the effect of N_L on the attachment kinetics of rat and of chicken hepatocytes to sugar-coated gels. They found that there is a critical N_L required for attachment of either cell type. In addition, the effect of an increase in N_L on the kinetics of rat hepatocyte attachment is similar to that predicted by our model. Edelman et al. (34) studied the effect of N_L on thymocyte attachment to lectin-coated fibers (serving as

TABLE 2 Comparison of probabilistic predictions for attachment to cell adhesion data

Predictions	Similar behavior (cell)
For shorter times, adhesive force increases with time	A–P
For longer times, rate of increase in adhesive force decreases and eventually reaches steady state	A; B; D; H–J; L–P
Attachment kinetics are a function of the ligand concentration	A; P
Attachment kinetics are a function of the affinity constant	Q
Time lag before onset of adhesion	B; C; F; G; M

(A) Rat hepatocyte adhesion to immobilized sugar (29); (B) Chicken hepatocyte adhesion to immobilized sugar (29); (C) Embryonic chicken (EmC) neural retina cell-to-cell adhesion (30); (D) EmC neural retina cell-to-cell adhesion (10); (E) EmC liver cell-to-cell adhesion (30); (F) Endothelial cell (EC) adhesion to various substrates (9); (G) EC adhesion to saline-treated glass (9)*; (H) EC adhesion to fibronectin-coated and to fibrinogen-coated glass (26); (I) EC adhesion to bovine serum albumin-coated glass (26)*; (J) EC adhesion to treated graft surfaces (19); (K) EC adhesion to untreated graft surfaces (19)*; (L) P388D1 mouse macrophage-like cell adhesion to glass (6)*; (M) MOPC 315 adhesion to fibronectin-coated vials (31); (N) CAC of tissue culture cells with lectin-coated surfaces (32); (O) CAC of mouse bone marrow cells with lectin-coated surfaces (33); (P) CAC of thymocytes with lectin-coated surfaces (34); (Q) Avidin-biotin immunosorption of Ia-positive cells (35, 36).
*Nonspecific adhesion

the affinity surface for CAC) as a function of time. Here, too, the kinetic behavior is consistent with that predicted by the attachment models. A decrease in κ can also result from an increase in K^o (increase in k_f^o and/or a decrease in k_r^o). Values for K^o, k_f^o, and k_r^o typically are unknown for adhesion receptors, making interpretation of attachment data for various receptor-ligand combinations difficult at this time. One exception is the CAC data of Berenson et al. (35, 36) for the interaction between TCs labeled with biotinylated antibodies and avidin-coated beads. The affinity constant for the reaction between avidin and biotin is extremely high, having a value of ~ 10 cm^2 (37). This value for K^o is much higher than that for other typical ligand-receptor interactions (order 10^{-11}–10^{-5} cm^2 [38]). Berenson et al. found that high TC adhesion efficiencies are obtained for avidin-biotin immunosorption without prolonged incubation of the TCs with the affinity surface. In fact, they used continuous flow through the column, whereas incubation periods on the order of 30 min are typical for separations with monoclonal antibody as ligand (8, 17, 18). These results suggest that an increase in K^o increases the initial rate of bond formation,

Predictions	Similar behavior (cell)
Detachment begins instantaneously	A–C; I
Detachment occurs over a period of time	A–C; H; I
Detachment rate decreases with time of shear (Fraction attached [ζ] becomes fairly constant)	A–C; H; I
Final value of ζ is function of shear stress (S)	G; H*; I
Initial detachment rate increases with S	I
Final value of ζ increases as ligand density increases	D–F

(A) Endothelial cell (EC) adhesion to fibronectin-coated grafts in vivo (39) and in vitro (40); (B) EC adhesion to uncoated grafts in vivo (39, 65) and in vitro (40)[‡]; (C) White blood cell (WBC) adhesion to anti-WBC antibody-coated beads (41); (D) Tumor cell depletion with CAC (42); (E) CAC of thymocytes or erythrocytes with lectin-coated surfaces (34); (F) Avidin-biotin immunosorption of spleen cells (43); (G) Avidin-biotin immunosorption of Ia-positive cells (35); (H) Embryonic chicken neural retina cell-to-cell adhesion (10); (I) P388D1 mouse macrophage-like cell adhesion to glass (6)[‡].
*Sigmoidal-shaped curve
[‡]Nonspecific adhesion

yielding a greater bond number at a given t_a; this is consistent with the predictions of the attachment model.

Detachment

Data from several different cell adhesion assays (see Table 3) show behavior that resembles that seen in the RFDA data (Fig. 3) and in the probabilistic analyses of detachment for inital probability distributions with a variance greater then zero (Part 1 [1], Fig. 8). Here, we discuss similarities seen for EC seeding of prosthetic vascular grafts and for CAC. Ramalanjaona et al. (39) studied in vivo EC detachment kinetics for fibronectin-coated and for uncoated grafts. For both coated and uncoated grafts, they found that detachment begins instantaneously, occurs over a period of time, and essentially stops at longer times, yielding a fairly constant value for the fraction of adherent ECs. In addition, they found that the inital rate of detachment decreases and the final fraction of adherent cells increases when the surface is coated with fibronectin (specific interaction). This EC detachment behavior was also seen in studies using an in vitro seeded graft assay with fibronectin-coated and uncoated grafts (40). These EC seeding data are consistent with the probabilistic detachment analysis.

Peterson (41) examined cell detachment kinetics in CAC for the interaction between white blood cells (WBCs) and anti-WBC antibody-coated beads. The cells were first incubated with the beads for 2 h, the beads with attached cells were then resuspended in cell-free medium, and detachment was measured as a function of time. Here, detachment was measured under the *same* conditions as attachment. He found that detachment begins instantaneously, the cells detach over a period of time, and the rate of detachment decreases with time, reaching a value close to zero for longer times. These data are consistent with the probabilistic detachment analysis. In addition, they demonstrate that even when a cell is adherent, there is a continuing probability that the bonds will break and the cell will detach.

The effect of various parameters on the TC removal (adhesion) efficiency in CAC has been examined by several investigators. Certain results are consistent with the predictions of the probabilistic detachment model (see Table 3). For example, Berenson et al. (35) examined the effect of flow rate on CAC removal efficiency for the interaction between Ia-positive cells labeled with biotinylated antibody and avidin-coated surfaces. They found similar adhesion efficiencies for flow rates between 0.75 and 1.5 ml/min; however, for flow rates >1.5 ml/min, the adhesion efficiency decreases as flow rate (shear stress) increases. Certain CAC data have shown that the adhesion efficiency increases as N_L increases, i.e., the final fraction of TC that remain attached (ζ_F or $P_{b(F)}$) increases as κ decreases (N_L increases). This behavior has been observed for the interaction between tumor cells (42) or spleen cells (43) labeled with biotinylated antibody and avidin-coated surfaces and between thymocytes or erythrocytes and lectin-coated surfaces (34). Here, we should mention that care should be taken to optimize N_L and attachment time because cells may modulate receptor expression on prolonged exposure to high N_L (20). In addition, an increase in TC receptor number has also been found to improve TC adhesion efficiencies (43, 44). Therefore, as predicted by the probabilistic model, the adhesion efficiency is optimized by decreasing the shear stress and/or increasing the receptor and/or ligand densities.

A high tumor cell removal efficiency is crucial for CAC because tumor cells can be clonogenic in vivo with only 0.0001% of the cells in the "cleansed" marrow (17). A problem with CAC is that tumor cell removal is frequently insufficient. Typically, this is attributed to tumor cell receptor heterogeneity and/or an inadequate tumor cell to ligand-coated bead ratio. Kvalheim et al. (18) investigated the effect of the tumor cell to immunobead ratio and of two cycles of treatment on TC removal efficiencies. They found that the removal efficiencies with a bead concentration of 1.8 mg/ml were inferior to those obtained with a concentration of 5.3 mg/ml or 8.9 mg/ml; the removal efficiencies were similar for concentrations of 5.3 mg/ml and 8.9 mg/ml; one cycle of treatment yielded

insufficient removal efficiencies; and two cycles of treatment improve TC removal efficiencies, yielding tumor cell percentages at or below 0.0001%. The similar removal efficiencies for bead concentrations of 5.3 and 8.9 mg/ml suggest that the inadequate removal efficiency for the first cycle of treatment is not the result of an improper bead to tumor cell ratio. The efficient removal in the second cycle suggests that inadequate removal in the first cycle cannot be completely attributed to receptor heterogeneity. These data are, however, consistent with our probabilistic analysis of detachment. Our model predicts that the final fraction of TC that remain attached (ζ_F) is not a function of the number of TCs in the marrow but the conditions of the separation, assuming that the surface is not limiting. In other words, if the conditions are such that 99.9% of the TC remain adherent, then we predict this to be the case regardless of whether the marrow is contaminated with 10% TC (as in the first cycle of Kvalheim et al.'s experiment) or with ~0.01% TC (as in the second cycle). This suggests that the use of consecutive cycles of treatment in CAC may be an effective means of reducing the final TC concentration. Here we should mention that other studies on CAC have also shown improved tumor cell removal efficiencies can be achieved by staging (17, 45).

In summary, the detachment data for both receptor-coated latex beads (prototype cells) and cells can be readily interpreted with the probabilistic models developed in Part 1 (1). This is not surprising because fluctuations are inherent to some degree in chemical reactions, especially when the number of reacting molecules is relatively small (46–48). The deterministic framework does not allow for deviations or fluctuations about the mean solution; therefore, it is difficult to interpret transient data solely on the basis of a deterministic analysis. In Part 1 we also show that care must be taken in using a deterministic model to predict detachment behavior, it can overestimate the force required to detach the cells and the time required for the cells to detach. In addition, a deterministic model does not predict partial detachment at the lower range of shear, detachment which may ruin the success of processes such as CAC and EC seeding. Finally, the similarity of the CAC and EC seeding data with the probabilistic predictions suggest that our probabilistic model can provide useful insight into the effect of various parameters on the optimization of target cell and EC adhesion efficiencies.

APPENDIX 1

Role of heterogeneity

In our analysis (1), we focus on the role of receptor-ligand kinetics in yielding deviations from ideal, deterministic behavior. A deterministic model does not provide for fluctuations about the mean solution. Fluctuations are, however, inherent to some degree in chemical reactions, especially when the number of reacting molecules is relatively small as is the case with the receptors on our model cells. Deviations from ideal behavior may, however, also result from heterogeneous properties, such as the Ag/Ab affinity constant and the number of Ag and of Ab available for binding within the contact area. Here, we compare the role of heterogeneity with that of the kinetics for our model bead system.

The probabilistic initial condition for detachment for our model cell system predicts a mean bond number ($\langle\theta\rangle$) of 0.84 and a variance (σ^2) of 0.13 (see Results and Discussion). The standard deviation (σ) is, therefore, 0.43, where this value has been normalized with respect to $\langle\theta\rangle$. This value for σ provides a measure of the contribution of the kinetics in yielding deviations from deterministic behavior, where the deterministic model predicts $\sigma = 0$. For the Ab-coated bead data, the typical number of active receptors per bead is ~4×10^5 (see Table 1). If we assume that the radius of the contact area (a) is 0.5 μm (see Results and Discussion), then the number of receptors available for binding within the contact area (R_T) is 1,000. In reality, R_T is probably best described as a Poisson distribution, rather than as uniform (49). The relative error in assuming a uniform distribution is, therefore, equal to $\langle R_T\rangle^{-0.5}$, where $\langle R_T\rangle$ is equal to the mean value of R_T. This error is equivalent to σ because θ is normalized with respect to R_T. For $\langle R_T\rangle = 1,000$, $\sigma = 0.03$. Using a smaller value for a of 0.25 μm, $\langle R_T\rangle = 250$ and $\sigma = 0.06$. Whereas these values for σ are not insignificant, they are both smaller than the contribution from the kinetics.

Next, we examine the net effect of heterogeneity in the ligand number and in the affinity constant on the heterogeneity of the dimensionless affinity constant (κ^{-1}). For the Ab-coated bead data, the typical value for the active ligand density is 5×10^{11} cm^{-2} (see Table 1). Assuming $a = 0.5$ μm, the number of ligand available for binding within the contact area is 4,000. As with R_T, the ligand number is probably best described as a Poisson distribution, rather than as uniform. For 4,000 molecules, the error in assuming a uniform distribution is 2%. For $a = 0.25$ μm, the number of ligand is 1,000 and the error is 3%. The Ab used in this work is a polyclonal antibody, therefore, the affinity constant is heterogeneous, typically described by a Gaussian or Sipsian distribution (50–52). We assume that only one binding site per Ab remains active, consistent with data reported by Clausen (53) on covalent coupling of IgG to a surface with glutaraldehyde; therefore, we do not expect the large variations in affinity that could occur if only certain Abs could form two bonds. From the estimates for the heterogeneity in the ligand number and from measurements of Pauling et al. (50) and of Nisonoff and Pressman (51) on the heterogeneity of polyclonal rabbit antibody, we estimate the standard deviation in the dimensionless affinity constant (κ^{-1}) for our Ag/Ab system is on the order of 0.05, where this value is normalized with respect to the mean value of 35 (see Results and Discussion). We must determine the effect of this value on the value for σ (the SD about $\langle\theta\rangle$), which can be obtained using Eq. 5 in Part 1 (1); we obtain a value for σ of 0.03. Therefore, σ from R_T heterogeneity is between 0.03 and 0.06 and from ligand number and affinity constant heterogeneities is 0.03, yielding a net value for σ of between 0.04 and 0.07, i.e., a contribution about an order of magnitude smaller than that of the kinetics. Therefore, we neglect the role of heterogeneities in yielding deviations from deterministic behavior, while recognizing that rigorous modeling of these data would also include these effects.

We can also use a qualitative comparison of the behavior predicted by the probabilistic model with that expected if the deterministic model were modified to account for heterogeneity in receptor number, ligand number, and affinity constant to justify our focus on the role of the kinetics. As demonstrated above, for the receptor and ligand numbers used in our experiments, the heterogeneity is relatively small; therefore, each bead would have approximately the same number of bonds. The Ab

is purchased from Sigma Immuno Chemicals (St Louis, MO) as affinity purified immunoglobulin, i.e., the Ab has been separated on the basis of its affinity for the Ag. Typically, this purification step will remove not only molecules that are not specific for the Ag, but also low affinity Ab (51). It is also important to remember that the heterogeneity in affinity is seen on the level of a given bead rather than on the level of the beads themselves. In other words, Abs within the contact area of a given bead have a range of affinities rather than each bead having a population of Abs with a given affinity. For a bead to detach, all of the bonds must break. The deterministic detachment analysis for our polyclonal Ab would, therefore, still predict that there is a time lag before the start of detachment, rather than that detachment begins instantaneously (as seen for our model cells [see Fig. 3] and as predicted by the probabilistic analysis of detachment with a variance greater than zero [Part 1 (1), Fig. 8]). To explain, initial bond distributions that include small values for the bond number yield detachment that begins instantaneously. These small values are obtained with the deterministic analysis for large κ, i.e, small K° (see Part I).

APPENDIX 2

Parameter estimation

Ligand density

N_L is estimated from the ligand concentration (L) of the coating solution as previously described (2).

Receptor-ligand affinity constant

Here, we assume $K^{\circ} \approx 6.9 \times 10^{-11}$ cm^2 for three reasons. First, Cozens-Roberts et al. (2) estimate that the affinity constant (K°) for the model cell system with the complementary antibodies used in the present experiments is of order 10^{-10} cm^2. Second, Perelson et al. (54) estimate that the affinity constant (K) of formation of the second bond between singly bound IgG immunoglobulin and surface-associated antigen is of order 10^{-10} cm^2. Singly bound IgG antibody is somewhat analogous to covalently coupled IgG antibody because only one additional bond can form and the realm of the active site is restricted. In addition, though less relevant to our system, experimentally measured values of the affinity constant for hapten-antibody reactions range between 10^{-12} and 10^{-2} cm^2 (55). Third, the analysis with this value yields results that are consistent with the RFDA kinetic data for both attachment and detachment.

Reverse rate constant

We assume that $k_r^{\circ} \approx 3.3 \times 10^{-5}$ s^{-1} (0.0020 min^{-1}). The bimolecular reaction between receptor and ligand can be modeled as a two-step process, where the first step is translational and orientational diffusion of the molecules to a position appropriate for reaction and the second step is the reaction itself (56, 57). k_r° (the overall reverse rate constant) can be expressed as (56, 57): $k_r^{\circ} = k_{-1}k_-/(k_1 + k_-)$, where k_- is the reverse diffusive rate constant and k_1 and k_{-1} are the forward and reverse intrinsic rate constants, respectively. Unlike the diffusive rate constants, the intrinsic rate constants are not a function of geometry (56, 57). In other words, the intrinsic rate constants for a given receptor-ligand system are the same whether the receptor is in solution, on the cell surface, or immobilized to a bead; the diffusive rate constants, however, are different in each case. For our case, immobilized receptor and immobilized ligand, k_- should be small; therefore, k_r° should also be small. As mentioned above, singly bound IgG antibody is similar to immobilized IgG antibody because only one additional bond can form and the realm of the active site is restricted. Here, we extend this

analogy further by assuming that k_r° for the bivalent interaction between IgG and surface-associated antigen is somewhat similar to k_r° for immobilized antibody and immobilized antigen. Data on k_r° for the interaction between IgG antibody and immobilized hapten yield values on the order of 10^{-3}–10^{-5} s^{-1} (58–61). These are typically several orders of magnitude lower than those for the antibody and hapten in solution (60). Theoretically, k_r° for the interaction between IgG antibody and surface-associated antigen is estimated to be of order 10^{-4}–10^{-5} s^{-1} (62), in excellent agreement with the available data. We assume that $k_r^{\circ} \approx 3.3 \times 10^{-5}$ s^{-1} because this value is within the range of measured and predicted values for the interaction between IgG antibody and surface-associated antigen and yields results that are consistent with the RFDA kinetic data for both attachment and detachment.

Forward rate constant

Here, we assume that $k_f^{\circ} \approx 1.4 \times 10^{-13}$ cm^2/min simply because

$$k_f^{\circ} = K^{\circ}k_r^{\circ}$$

APPENDIX 3

Estimation of settling velocity

Using Stokes' Law, we estimate the settling time for beads in the RFDA to be between 0 (beads on the affinity surface at $t_a = 0$) and 1.5 min (beads at the top of the gap at $t_a = 0$). Stokes' Law, however, provides only an approximation for the settling time because it applies to the ideal case of a sphere sedimenting through a viscous fluid that extends to infinity in all directions (63). Brenner's (64) "exact" solution for the movement of a solid sphere toward a rigid plane surface predicts that the settling velocity is less than that predicted by Stokes' Law. The explanation is that the velocity decreases as the sphere approaches the surface (instead of remaining constant as predicted by Stokes' Law) due to friction between the fluid and the surface which slows the rate at which fluid is displaced from the path of the approaching bead (18, 64). Brenner accounts for this effect by multiplying the expression for the frictional force by a correction factor, $\lambda(\rho_B/x)$, where x is the separation distance between the bead and plate. At small ρ_B/x (large separation distances), $\lambda \approx 1$, whereas at large ρ_B/x, $\lambda \approx \rho_B/x$ (15, 64). Another factor that could increase the settling time is the transient period required for the particle to reach terminal velocity (63); the model "cells" are, however, predicted to reach terminal velocity almost instantaneously.

REFERENCES

1. Cozens-Roberts, C., J. A. Quinn, and D. A. Lauffenburger. 1990. Receptor-mediated cell attachment and detachment kinetics. I.

Probabilistic model and analysis. *Biophysical Journal.* 58:841–856.

2. Cozens-Roberts, C., J. A. Quinn, and D. A. Lauffenburger. 1990. Receptor-mediated adhesion phenomena. Model studies with the Radial-Flow Detachment Assay. *Biophys. J.* 58:107–125.

3. Bongrand, P., C. Capo, A. M. Benoliel, and R. Depieds. 1979. Evaluation of intercellular adhesion with a very simple technique. *J. Immunol. Methods.* 28:133–141.

4. Capo, C., F. Garrouste, A. Benoliel, P. Bongrand, A. Ryter, and G. I. Bell. 1982. Concanavalin-A-mediated thymocyte agglutination: a model for a quantitative study of cell adhesion. *J. Cell Sci.* 56:21–48.

5. Pelton, R. H., and L. H. Allen. 1984. Factors influencing the adhesion of polystyrene spheres attached to pyrex by polyethyleneimine in aqueous solution. *J. Colloid Interface Sci.* 99:387–398.

6. Mege, J. L., C. Capo, A. M. Benoliel, and P. Bongrand. 1986. Determination of binding strength and kinetics of binding initiation: a model study made on the adhesive properties of P388D1 macrophage-like cells. *Cell. Biophys.* 8:141–160.

7. Cress, M. C., and T. T. Ngo. 1989. Site specific immobilization of immunoglobulins. *Am. Biotechnol. Lab.* 7:16–19.

8. Berenson, R. J., L. J. Levitt, R. Levy, and R. A. Miller. 1984. Cellular immunosorption using monoclonal antibodies. *Transplantation. (Baltimore).* 38:136–143.

9. Pratt, K. J., B. E. Jarrell, S. K. Williams, R. A. Carabasi, M. A. Rupnick, and M. A. Hubbard. 1988. Kinetics of endothelial cell-surface attachment forces. *J. Vasc. Surg.* 7:591–599.

10. McClay, D. R., G. M. Wessel, and R. B. Marchase. 1981. Intercellular recognition: quantitation of initial binding events. *Proc. Natl. Acad. Sci. USA.* 78:4975–4979.

11. Crouch, C. F., H. W. Fowler, and R. E. Spier. 1985. The adhesion of animal cells to surfaces: the measurement of critical surface shear stress permitting attachment or causing detachment. *J. Chem. Technol. Biotechnol.* 35B:273–281.

12. Bell, G. I. 1978. Models for the specific adhesion of cells to cells. *Science (Wash. DC).* 200:618–627.

13. Hammer, D. A., and D. A. Lauffenburger. 1987. A dynamic model for receptor-mediated cell adhesion to surfaces. *Biophys. J.* 52:475–487.

14. Ottewill, R. H. 1977. Stability and instability in disperse systems. *J. Colloid Interface Sci.* 58:357–373.

15. Ruckenstein, E., and D. C. Prieve. 1975. Dynamics of deposition on surfaces. *J. Theor. Biol.* 51:429–438.

16. Bongrand, P., and G. I. Bell. 1984. Cell-cell adhesion: parameters and possible mechanisms. *In* Cell Surface Dynamics: Concepts and Models. A. S. Perelson, C. DeLisi, and F. W. Wiegel, editors. Marcel Dekker, Inc., New York. 459–493.

17. Seeger, R. C., D. D. Vo, J. Ugelstad, and C. P. Reynolds. 1986. Removal of neuroblastoma cells from bone marrow with monoclonal antibodies and magnetic immunobeads. *In* Transfusion Medicine: Recent Technological Advances. K. Murawski and F. Peetoom, editors. Alan R. Liss, Inc., New York. 285–293.

18. Kvalheim, G., O. Fodstad, A. Pihl, K. Nustad, A. Pharo, J. Ugelstad, and S. Funderud. 1987. Elimination of B-lymphoma cells from human bone marrow: model experiments using monodisperse magnetic particles coated with primary monoclonal antibodies. *Cancer Res.* 47:846–851.

19. Jarrell, B. E., S. K. Williams, L. Solomon, L. Speicher, E. Koolpe, J. Radomski, R. A. Carabasi, D. Greener, and F. E. Rosato. 1986. Use of an endothelial monolayer on a vascular graft prior to implantation. *Ann. Surg.* 203:671–678.

20. Estrabrook, A., C. L. Berger, R. Mittler, P. LoGerfo, M. Hardy, and R. L. Edelson. 1983. Antigenic modulation of human T-lymphocytes by monoclonal antibodies. *Transplant. Proc.* 15:651–656.

21. Martin, P. J., E. R. Giblett, and J. A. Hansen. 1982. Phenotyping human leukemic T-cell lines: enzyme markers, surface antigens, and cytogenetics. *Immunogenetics.* 15:385–398.

22. Pratt, B. M., D. Forn, and J. A. Madri. 1985. Endothelial cell-extracellular matrix interactions. *Ann. NY Acad. Sci.* 460:274–288.

23. Albelda, S. M., M. Daise, E. N. Levine, and C. A. Buck. 1989. Identification and characterization of cell-substratum adhesion receptors on cultured human endothelial cells. *J. Clin. Invest.* 83:1992–2002.

24. Hafeman, D. G., V. von Tscharner, and H. M. McConnell. 1981. Specific antibody-dependent interactions between macrophages and lipid haptens in planar lipid monolayers. *Proc. Natl. Acad. Sci. USA.* 78:4552–4556.

25. Wilkinson, P. C., J. M. Lackie, J. V. Forrester, and G. A. Dunn. 1984. Chemokinetic accumulation of human neutrophils on immune complex-coated substrata: analysis at a boundary. *J. Cell Biol.* 99:1761–1768.

26. Dejana, E., S. Colella, L. R. Languino, G. Balconi, G. C. Corbascio, and P. C. Marchisio. 1987. Fibrinogen induces adhesion, spreading, and microfilament organization of human endothelial cells in vitro. *J. Cell Biol.* 104:1403–1411.

27. Eskin, S. G., C. L. Ives, L. V. McIntire, and L. T. Navarro. 1984. Response of cultured endothelial cells to steady flow. *Microvasc. Res.* 28:87–94.

28. Sung, K. P., L. A. Sung, M. Crimmins, S. J. Burakoff, and S. Chien. 1986. Determination of junction avidity of cytolytic T cell and target cell. *Science (Wash. DC).* 234:1405–1408.

29. Weigel, P. H., R. L. Schnaar, M. S. Kuhlenschmidt, E. Schmell, R. T. Lee, Y. C. Lee, and S. Roseman. 1979. Adhesion of hepatocytes to immobilized sugars, a threshold phenomenon. *J. Biol. Chem.* 254:10830–10838.

30. Umbreit, J., and S. Roseman. A Requirement for reversible binding between aggregating embryonic cells before stable adhesion. *J. Biol. Chem.* 250:9360–9368.

31. Liao, N., J. St. John, Z. J. Du, and H. T. Cheung. 1987. Adhesion of lymphoid cell lines to fibronectin-coated substratum: biochemical and physiological characterization and the identification of a 140-kDa fibronectin receptor. *Exp. Cell Res.* 171:306–320.

32. Kinzel, V., J. Richards, and D. Kubler. 1977. Lectin receptor sites at the cell surface employed for affinity separation of tissue culture cells. *Exp. Cell Res.* 105:389–400.

33. Nicola, N. A., A. W. Burgess, D. Metcalf, and F. L. Battye. 1978. Separation of mouse bone marrow cells using wheat germ agglutinin affinity chromatography. *Aust. J. Exp. Biol. Med. Sci.* 56:663–679.

34. Edelman, G. M., U. Rutishauser, and C. F. Millette. 1971. Cell fractionation and arrangement on fibers, beads, and surfaces. *Proc. Natl. Acad. Sci. USA.* 68:2153–2157.

35. Berenson, R. J., W. I. Bensinger, and D. Kalamasz. 1986. Positive selection of viable cell populations using avidin-biotin immunoadsorption. *J. Immunol. Methods.* 91:11–19.

36. Berenson, R. J., W. I. Bensinger, D. Kalamasz, F. Schuening, H. J. Deeg, T. Graham, and R. Storb. 1987. Engraftment of dogs with Ia-positive marrow cells isolated by avidin-biotin immunoadsorption. *Blood.* 5:1363–1367.

37. Bayer, E. A., and M. Wilchek. 1980. The use of the avidin-biotin complex as a tool in molecular biology. *Methods Biochem. Anal.* 26:1–45.

38. Bell, G. I., M. Dembo, and P. Bongrand. 1984. Cell adhesion: competition between nonspecific repulsion and specific bonding. *Biophys. J.* 45:1051–1064.

39. Ramalanjaona, G., R. F. Kempczinski, J. E. Rosenman, C. Douville, and E. B. Silberstein. 1986. The effect of fibronectin coating on endothelial cell kinetics in polytetrafluoroethylene grafts. *J. Vasc. Surg.* 3:264–272.

40. Kesler, K. A., M. B. Herring, M. P. Arnold, J. L. Glover, H. M. Park, M. N. Helmus, and P. J. Bendick. 1986. Enhanced strength of endothelial attachment on polyester elastomer and polytetrafluoroethylene graft surfaces with fibronectin substrate. *J. Vasc. Surg.* 3:58–64.

41. Peterson, D. R. 1987. Cell fractionation techniques. *DuPont Magazine-College Report.* May/June: Centerfold.

42. Berenson, R. J., W. I. Bensinger, D. Kalamasz, and P. Martin. 1986. Elimination of daudi lymphoblasts from human bone marrow using avidin-biotin immunosorption. *Blood.* 67:509–515.

43. Basch, R. S., J. W. Berman, and E. Lakow. 1983. Cell separation using positive immunoselective techniques. *J. Immunol. Methods.* 56:269–280.

44. Rutishauser, U., and L. Sachs. 1975. Receptor mobility and the binding of cells to lectin-coated fibers. *J. Cell Biol.* 66:76–85.

45. Kvalheim, G., J. G. Field, A. Pihl, S. Funderud, J. Ugelstad, O. Fodstad, and K. Nustad. 1989. Immunomagnetic removal of B-lymphoma cells using a novel mono-sized magnetizable polymer bead, M-280, in conjunction with primary IgM and IgG antibodies. *Bone Marrow Transplant.* 4:567–574.

46. McQuarrie, D. A. 1963. Kinetics of small systems. I. *J. Chem. Phys.* 38:433–436.

47. McQuarrie, D. A. 1964. Kinetics of small systems. II. *J. Chem. Phys.* 40:2914–2921.

48. Bartholomay, A. F. 1962. A stochastic approach to statistical kinetics with application to enzyme kinetics. *Biochemistry.* 1:223–230.

49. Berg, H. C. 1983. Random Walks in Biology. Princeton University Press, Princeton, NJ. 142 pp.

50. Pauling, L., M. D. Pressman, and A. L. Grossberg. 1944. The serological properties of simple substances. VII. A quantitative theory of the inhibition by haptens of the precipitation of heterogeneous antisera with antigens, and comparison with experimental results for polyhaptenic simple substances and for azoproteins. *J. Am. Chem. Soc.* 66:784–792.

51. Nisonoff, A., and D. Pressman. 1958. Heterogeneity and average combining constants of antibodies from individual rabbits. *J. Immunol.* 80:417–428.

52. Sada, E., S. Katoh, K. Sukai, M. Tohma, and A. Kondo. 1986. Adsorption equilibrium in immuno-affinity chromatography with polyclonal and monoclonal antibodies. *Biotechnol. Bioeng.* 28:1497–1502.

53. Clausen, J. 1981. Immunochemical techniques for the identification and estimation of macromolecules. *In* Laboratory Techniques in Biochemistry and Molecular Biology. T. S. Work and E. Work, editors. North-Holland Publishing Co., New York. 387 pp.

54. Perelson, A. J., B. Goldstein, and S. Rocklin. 1980. Optimal strategies in immunology III. The IgM-IgG switch. *J. Math. Biol.* 10:209–256.

55. Pecht, I., and D. Lancet. 1977. Kinetics of antibody-hapten interactions. *Mol. Biol. Biochem. Biophys.* 24:306–338.

56. Lauffenburger, D., and C. DeLisi. 1983. Cell surface receptors: physical chemistry and cellular regulation. *Int. Rev. Cytol.* 84:269–302.

57. DeLisi, C. 1980. The biophysics of ligand-receptor interactions. *Q. Rev. Biophys.* 13:201–230.

58. Hornick, C. L., and F. Karush. 1969. The interaction of hapten-coupled bacteriophage ϕX174 with antihapten antibody. *Isr. J. Med. Sci.* 5:163–170.

59. Hornick, C. L., and F. Karush. 1972. Antibody affinity—III The role of multivalency. *Immunochemistry.* 9:325–340.

60. Karush, F. 1978. The affinity of antibody: range, variability, and the role of multivalence. *In* Immunoglobulins. G. W. Litman and R. A. Good, editors. Plenum Medical Book Company, New York. 85–116.

61. Nygren, H., M. Kaartinen, and M. Stenberg. 1986. Determination by ellipsometry of the affinity of monoclonal antibodies. 1986. *J. Immunol. Methods.* 92:219–225.

62. Stenberg, M., L. Stibert, and H. Nygren. 1986. External diffusion in solid-phase immunoassays. *J. Theor. Biol.* 120:129–140.

63. Denn, M. M. 1980. Process Fluid Mechanics. Prentice-Hall, Inc., Englewood Cliffs, NJ. 383 pp.

64. Brenner, H. 1961. The slow motion of a sphere through a viscous fluid towards a plane surface. *Chem. Eng. Sci.* 16:242–251.

65. Rosenman, J. E., R. F. Kempczinski, W. H. Pearce, and E. B. Siberstein. 1985. Kinetics of endothelial seeding. *J. Vasc. Surg.* 2:778–784.